WIND ENERGY
Wind Energ. 2011; **14**:209–224
Published online 26 August 2010 in Wiley Online Library (wileyonlinelibrary.com). DOI: 10.1002/we.413

RESEARCH ARTICLE

Effect of steady deflections on the aeroelastic stability of a turbine blade

B. S. Kallesøe

Wind Energy Department, Risø-DTU, Technical University of Denmark, DK-4000 Roskilde, Denmark

ABSTRACT

This paper deals with effects of geometric non-linearities on the aeroelastic stability of a steady-state deflected blade. Today, wind turbine blades are long and slender structures that can have a considerable steady-state deflection which affects the dynamic behaviour of the blade. The flapwise blade deflection causes the edgewise blade motion to couple to torsional blade motion and thereby to the aerodynamics through the angle of attack. The analysis shows that in the worst case for this particular blade, the edgewise damping can be decreased by half. Copyright © 2010 John Wiley & Sons, Ltd.

KEYWORDS

stability analysis; aeroelasticity

Correspondence

B. S. Kallesøe, Wind Energy Division, Risø DTU, Frederiksborgvej 399, P.O. Box 49, DK-4000 Roskilde, Denmark.
E-mail: bska@risoe.dtu.dk

Received 5 October 2009; Revised 17 May 2010; Accepted; 31 May 2010

1. INTRODUCTION

A second-order non-linear beam model is used for aeroelastic stability analysis of a wind turbine blade. The importance of including the effects of non-linear geometric couplings in the stability analysis is considered and the aeroelastic mechanisms driving the aeroelastic response are described in detail.

The effect of non-linear geometric couplings in a curved rotating blade on the stability has been investigated in the helicopter society for decades[1–4] and state-of-the-art comprehensive helicopter stability codes of today, like Hodges *et al.*,[5] include both material and geometric non-linearities. However, most aeroelastic stability tools for wind turbines are based on linear beam theory and do not include the non-linear geometric coupling caused by, for instance, steady-state blade deflection, pre-bend or swept blade.

In the late 1970s, the oil crisis stimulated many MW size turbine projects. In a review of research on aeroelastic stability Friedmann[6] concluded that '*Reliable aeroelastic stability analyses should be based on non-linear formulations which account for both moderately large deformations (i.e. finite slopes) and non-linear aerodynamic effects, such as stall*'. All these MW size turbine projects however ended without any commercial success. Later, the wind turbine followed a development starting at small 30 kW units gradually growing to today's MW size commercial turbine. During this period, wind turbines have been relatively stiff constructions with only limited geometric couplings. Chaviaropoulos[7] examines the influence of non-linear effects on the aeroelastic stability of a 19 m blade. It was found that the most important effect to include is the unsteady aerodynamics and that the structural deflection is unimportant. Modern wind turbine blades are longer (up to 60 m) and more slender, thus increasing the blade deflection under normal operation and thereby reintroducing stability issues concerning geometric couplings. Steady-state blade deflection will result in geometrically non-linear couplings between the different blade modes. For instance, a large flapwise blade deflection will enhance the coupling between edgewise and torsional blade motion and consequently affect the aerodynamics through the angle of attack. Therefore, it can be important to include the non-linear geometric coupling between for example edgewise and torsional motion of a flapwise deflected blade.

Research in utilizing sweep and pre-bend blades is ongoing. The European Union founded project UPWIND[8–10] deals, among other issues, with non-linear modelling of blades and the effects of including such non-linearities. Some state-of-the-art stability codes, such as TURBU,[11] include the effect of geometric non-linearities. Riziotis *et al.*[12] include these effects in a stability analysis of a turbine in closed-loop operation. There is also focus on utilizing the geometric couplings to reduce fatigue and/or ultimate loads, for instance Ashwill *et al.*,[13] where a blade is swept to introduce a flapwise—torsion coupling.

Wind turbine stability can be analysed by a variety of different model types. The most detailed description of the turbine response is given by numerical non-linear time simulation tools.[14–18] These tools show instabilities as well as non-linear effects limiting the response to for instance limit cycle oscillations. They can also be used to analyse the effect of, for instance, turbulence and wind shear's effects on turbine stability. The referenced tools use different models and different model complexity. For instance, FAST[18] is a modal-based code which on the one hand does not include a torsional degree of freedom of the blade and non-linear geometric couplings, but on the other hand is relatively computationally inexpensive. A code like HAWC2[14,15] has a more complex model with a structural model based on a multi-body formulation where each body is a Timoshenko beam element including torsion. The drawback of these time-simulation tools is that they are computationally intensive and they can make it difficult to extract the important aeroelastic mechanisms from the large volume of results. Another approach is to use eigenvalue analysis of a linear (or linearized) model of the turbine.[11,12,19–21] The HAWCStab code[19,21] offers a platform for linearization of the undeflected turbine structure, while the code TURBU[11] offers a platform for aeroservoelastic stability analysis based on linearization around the deflected/curved blade state. The structural model in TURBU is based on a simple co-rotational beam element approach. Each beam element consists of a rigid body with springs and dampers in its entry point; average strains in the springs and torque-free rotation offsets between the beam elements embody the average deflected/curved blade state. Riziotis *et al.*[12] offers a multi-body platform which finds a reference state by time integration and linearizes the aeroservoelastic equations around this reference state to provide a stability tool including closed loop control. This type of tool can give both structural eigenfrequencies and eigenmodes that describe the basic structural dynamics of the turbine and aeroelastic frequencies, damping and modes of the aeroelastic motion. The aeroelastic damping reveals any stability problems for the turbine. However, since it is linear tools, they do not give any information concerning non-linear mechanism that limit the amplitude of a linear negative damped mode. The knowledge of structural and aeroelastic frequencies and mode shapes is very useful in the analysis and in the interpretation of results from aeroelastic time simulations. However, the modes of the aeroelastic response of the whole turbine can still be complex to analyse. To reduce the complexity, and thus make the results more transparent, a blade-only analysis is used.[22] This allows a clear physical interpretation and insight into the mechanisms that govern the dynamic response of the blade and many basic characteristic of turbine stability can be extract from a blade-only analysis.

This paper uses a non-linear blade model[23] which includes the effect of large blade deflections, pitch action and rotor speed variations. This blade model is strongly inspired by the work of Hodges and Dowell[1] First, the structural model is combined with a steady-state aerodynamic model based on beam element momentum (BEM) theory and discritized by a finite difference scheme. The resulting algebraic non-linear aeroelastic model is employed to compute steady-state blade deflections and induced velocities of a blade from the 5 MW Reference Wind Turbine (RWT) by National Renewable Energy Laboratory (NREL)[24] at normal power production conditions. The steady-state deflections are compared with the results from HAWC2 simulations, showing good agreement. Throughout this paper, the 5 MW RWT by NREL is used as an example blade. The reference turbine is an artificial turbine based on state-of-the-art turbines on the market. The blade is strongly inspired by the 61.5 m LM glasfiber blade (LM Wind Power, Kolding, Denmark). This blade belongs to the mid-region of flexible designs of state-of-the-art blades, and hence, the geometric couplings can be more pronounced for other blade designs. The big advantage of this blade however is that all data is publicly available and it has been widely used in other research work and therefore a good reference with realistic flexibility compared with most state-of-the-art blades. A non-linear structural blade model[23] and an unsteady aerodynamic model[25] are then linearized about the steady-state deflected blade, preserving the main effects of the geometric non-linearities. The linear model is discritized by the finite difference scheme which along with boundary conditions form a differential eigenvalue problem. The solution to this eigenvalue problem gives the aeroelastic frequencies and damping, but also information concerning the fundamental aeroelastic behaviour of the blade. The analysis shows that the aeroelastic damping of the edgewise modes changes when the steady-state deflection is included. The aeroelastic motion is analysed in detail for three different operation conditions in which there is large differences in the damping when including or excluding steady-state blade deflections.

2. STRUCTURAL BLADE MODEL

The structural blade model described in Kallesøe[23] is based on the work by Hodges and Dowell[1] using second-order Bernoulli–Euler beam theory to describe the blade motion by a non-linear partial integral-differential equation of motion

Wind Energ. 2011; **14**:209–224 © 2010 John Wiley & Sons, Ltd.
DOI: 10.1002/we

$$\bar{\mathbf{M}}\ddot{\bar{\mathbf{u}}} + \bar{\mathbf{F}}\left(\ddot{\bar{\mathbf{u}}}, \bar{\mathbf{u}}'', \bar{\mathbf{u}}', \bar{\mathbf{u}}, \ddot{\beta}, \dot{\beta}, \beta, \ddot{\phi}, \dot{\phi}, \phi\right) = \bar{\mathbf{f}}\left(\mathbf{f}_{aero}, M_{aero}, u', v'\right) \tag{1}$$

where $\bar{\mathbf{M}}$ is the mass matrix, $\bar{\mathbf{F}}$ is a non-linear function that includes stiffness, damping, gyroscopic terms together with centrifugal force-based integral terms. The state vector $\bar{\mathbf{u}} = [u\,(t, s), v\,(t, s), \theta\,(t, s)]$ holds edgewise, flapwise and torsional deformations, respectively.

Flapwise is defined as the direction normal to the rotor plane (positive downwind) and edgewise as in the rotor plane (positive towards leading edge) for a blade at zero pitch. When the blade pitches, the (u, v) frame follows the blade. The position along the blades elastic axis is denoted s, t is the time, $\beta = \beta(t)$ is the global pitch of the blade, $\phi = \phi(t)$ is the azimuth angle of the rotor and the right hand side force function $\bar{\mathbf{f}}$ holds the effect of the aerodynamic forces $\mathbf{f}_{aero}$ and aerodynamic moment M_{aero} on the blade. The dots denote time derivatives and the primes denote derivatives with respect to the longitudinal coordinate s. As an example, the equation of motion for edgewise blade bending is given by

$$\begin{aligned} &m\left(\ddot{u} - \ddot{\theta} l_{cg}\sin\left(\bar{\theta}\right)\right) + F_{u,1}\left(\ddot{\beta}, \dot{\beta}, \dot{\phi}, \dot{v}, \dot{\theta}, u', u, \theta, \beta\right) + F_{u,2}\left(\dot{\phi}, \dot{u}, \dot{v}, u', v, \theta, \beta\right) \\ &\quad + F_{u,3}(\phi, \beta, \theta, u', v') + F_{u,4}(u'', v'', \theta) + F_{u,5}\left(\ddot{\phi}, \beta\right) \\ &\quad = f_u + \left(\left(u' + l_{pi}'\right)\int_s^R f_w \mathrm{d}\rho\right)' \end{aligned} \tag{2}$$

where the first term is the inertia forces, the second term $F_{u,1}$ describes the influence of pitch action, which will not be used in this work. The third term $F_{u,2}$ describes centrifugal and Coriolis forces caused by the rotor speed. The fourth term $F_{u,3}$ describes the unsteady influence form gravity, which is neglected in this work. The fifth term describes the restoring forces

$$\begin{aligned} F_{u,4} = &\left(E\left(I_\xi \cos^2\left(\tilde{\theta}\right) + I_\eta \sin^2\left(\tilde{\theta}\right)\right)u''\right)'' + \left(E(I_\xi - I_\eta)\cos\left(\tilde{\theta}\right)\sin\left(\tilde{\theta}\right)v''\right)'' \\ &- \left(E(I_\xi - I_\eta)\theta\left(u''\sin\left(2\tilde{\theta}\right) - v''\cos\left(2\tilde{\theta}\right) + l_{pi}''\sin\left(\tilde{\theta}\right)\cos\left(\tilde{\theta}\right)\right)\right)'' \end{aligned} \tag{3}$$

where the first term is the bending stiffness in the x-direction, the second term is the coupling to the y-direction and the last term in equation (3) is the coupling to the twist. The sixth term in equation (2) describes the influence of rotor speed variations, which is assumed constant in this work, so the term is not active. The right hand side holds the external forces, which in this case will be aerodynamic forces. Longitudinal forces on and in the blade, for example the centrifugal force, lead to integral terms in the equations of motion. A detailed description of all terms are found in Kallesøe.[23]

The boundary conditions employed in this paper are for simplification derived for blades without pre-curvature. The boundary conditions for the root of the blade are given by the geometric constraints

$$u(0, t) = u'(0, t) = v(0, t) = v'(0, t) = \theta(0, t) = 0 \tag{4}$$

because the frame used to describe the blade follows the root of the blade.

The boundary conditions for the tip of the blade are[23]

$$\begin{aligned} &u''(R, t) = v''(R, t) = \theta'(R, t) = 0 \\ &u'''(R, t) = \frac{ml_{cg}}{EI_\xi I_\eta}\left(\dot{\phi}^2 w - g\cos(\phi)\right)\left(I_\eta \sin\left(\tilde{\theta} - \bar{\theta}\right)\sin\left(\tilde{\theta}\right) + I_\xi \cos\left(\tilde{\theta} - \bar{\theta}\right)\cos\left(\tilde{\theta}\right)\right) \\ &v'''(R, t) = \frac{ml_{cg}}{EI_\xi I_\eta}\left(\dot{\phi}^2 w - g\cos(\phi)\right)\left(I_\eta \cos\left(\tilde{\theta} - \bar{\theta}\right)\sin\left(\tilde{\theta}\right) + I_\xi \sin\left(\tilde{\theta} - \bar{\theta}\right)\cos\left(\tilde{\theta}\right)\right) \end{aligned} \tag{5}$$

where $s = R$ is the tip of the blade, $m = m(s)$ is the mass per length of the blade, $l_{cg} = l_{cg}(s)$ is the offset of centre of gravity from the elastic axis, $E = E(s)$ is the Young's modulus, $I = I\,(s)$ and $I_\eta = I_\eta(s)$ is the principle moments of inertia, $w = w(s, t)$ is the radius to the position s on the elastic axis, g denotes gravity, $\tilde{\theta} = \tilde{\theta}\,(s)$ is the angle between chord and principle axis of elasticity and $\tilde{\theta} = \tilde{\theta}\,(s)$ is the angle between the chord and a line between elastic centre and centre of gravity along which l_{cg} is measured. In the case that $l_{cg}(R) \neq 0$ the boundary conditions for the tip are functions of the rotor speed $\dot{\phi}$ and the azimuth angle of the rotor ϕ and therefore time varying. This is because an offset of the centre of gravity from the elastic axis at the blade tip leads to a bending moment at the tip caused by gravity and centrifugal force. Most modern wind turbine blades are tapered at the tip, whereby $l_{cg}(s) \xrightarrow[s\to R]{} 0$ and $EI_\xi I_\eta \xrightarrow[s\to R]{} 0$. Hence, it depends on the individual blade design if this azimuth angle-dependent boundary conditions can be neglected or not. In this work, the blade is constructed such that $l_{cg}(R) = 0$ and $EI_\xi I_\eta|_{s=R} \neq 0$, thus making the boundary conditions azimuth angel independent and hence all right hand sides of equation (5) become zero.

3. STEADY–STATE AEROELASTIC MODEL

To determine the steady-state deflection for the blade, a non-linear steady-state aeroelastic model is derived. Steady-state conditions are defined as uniform inflow, zero gravity, constant rotor speed and pitch angle $\ddot{\phi} = \dot{\beta} = 0$ whereby all time derivatives in the structural equations of motion (1) become zero $\ddot{u} = \ddot{v} = \ddot{\theta} = \dot{u} = \dot{v} = \dot{\theta} = 0$. These uniform conditions remove the periodicity of the system. The steady-state aerodynamic model is based on blade element momentum (BEM) theory including Prendtl's tip loss correction.[26] The BEM theory computes a balance between the forces on the blade and the momentum change in the wind. The aerodynamic model is coupled to the structural model through the local wind speed and angle of attack and the structural model is coupled to the aerodynamic model through the aerodynamic forces acting on the blade.

3.1. Discretization of structural model

The equations of motion (equation (1)) are discretized on an equidistant grid along the elastic axis with step size h and N computation points. The spatial derivatives of the partial differential equation of motion (1) are approximated by the finite difference scheme given in Table I. The derivatives of parameters (such as mass, stiffness, etc.) are approximated by the same finite difference scheme. The integral terms in the equation of motion are approximated by sums using the trapezoid rule.

The boundary conditions for the finite difference formulation are derived by inserting the finite difference approximations into the boundary conditions (equations (4) and (5)). It is assumed that the offset of the centre of gravity is zero at the blade tip, thus making the boundary condition independent of rotor position.

The discretized version of the partial differential equations of motion implemented on the N discretization points forms a set of non-linear algebraic equations:

$$\mathbf{F}_{st}(\mathbf{u}_0, \dot{\phi}_0, \beta_0) = \mathbf{f}_0 \tag{6}$$

where $\mathbf{F}_{st}$ ($\mathbf{u}_0$, $\dot{\phi}_0$, β_0) holds the terms from the discretization of the structural equation and $\mathbf{u}_0 = [u_{0,1}, v_{0,1}, \theta_{0,1}, \ldots, u_{0,N}, v_{0,N}, \theta_{0,N}]^T$ holds the steady-state deformation at each discretization point. The first subscript 0 denotes that it is the steady-state solution (zero order) and the second subscript denotes the discretization point, counting from the root of the blade. The right hand side $\mathbf{f}_0$ holds the steady-state aerodynamic forces computed at each discretization point using BEM theory.

3.2. Solution scheme

The finite difference discretized steady-state equation (equation (6)) has 3N unknown blade deflections (flapwise, edgewise and torsional deflections of the N discretization points) and 2N unknown induction factors (longitudinal and tangential induction factor at the N discretization points). This system of non-linear equations is solved using the following iterative scheme: i) Operational conditions are chosen: steady-state wind speed (U_0), the corresponding rotor speed $\dot{\phi}_0 = \dot{\phi}_0(U_0)$) and pitch setting ($\beta_0 = \beta_0(U_0)$); ii) apparent wind speed and angle of attack based on inflow conditions, blade deflections and induction factors are computed; iii) the aerodynamic forces using BEM theory are computed; iv) equation (6) is solved for the deformations $\mathbf{u}_0$; v) new induction factors are computed; and vi) if no convergence return to step 2. This gives the steady-state deformations $\mathbf{u}_0 = \mathbf{u}_0(U_0, \dot{\phi}_0, \beta_0)$ and the induction factors for the given operational condition.

Table I. Second-order finite difference formulation for uniform step size.

$f'(s, t)$	$\frac{\partial f(s,t)}{\partial s}$	$\frac{f_{i+1}(t) - f_{i-1}(t)}{2h}$
$f''(s, t)$	$\frac{\partial^2 f(s,t)}{\partial s^2}$	$\frac{f_{i+1}(t) - 2f_i(t) + f_{i-1}(t)}{h^2}$
$f'''(s, t)$	$\frac{\partial^3 f(s,t)}{\partial s^3}$	$\frac{-f_{i-2}(t) + 2f_{i-1}(t) - 2f_{i+1}(t) + f_{i+2}(t)}{2h^3}$
$f''''(s, t)$	$\frac{\partial^4 f(s,t)}{\partial s^4}$	$\frac{f_{i-2}(t) - 4f_{i-1}(t) + 6f_i(t) - 4f_{i+1}(t) + f_{i+2}(t)}{h^4}$

Wind Energ. 2011; **14**:209–224 © 2010 John Wiley & Sons, Ltd.
DOI: 10.1002/we

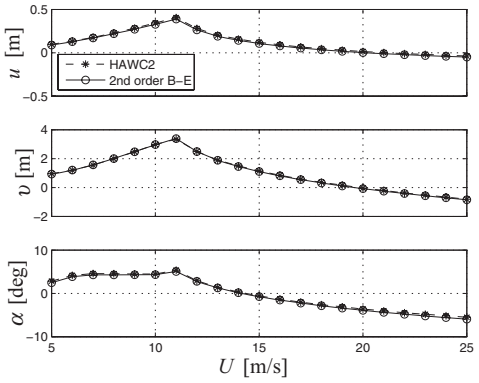

Figure 1. Edgewise and flapwise deflection and angle of attack at 55.5 m radius (88%) vs. wind speed for the present second-order Bernoulli–Euler blade model (equation (6)) and the non-linear aeroelastic time simulation code HAWC2.

3.3. Steady–state blade deflection at power production conditions

The steady-state model (equation (6)) is used to compute steady-state blade deflection and induction factors for the NREL 5 MW RWT[24] blade at normal power production operation. The results are compared with results from the non-linear aeroelastic time simulation code HAWC2.[14,15] The HAWC2 code is a multi-body formulation where each body is a linear Timoshenko beam element with a torsional degree of freedom. The geometric non-linearities are captured by the multi-body formulation, in which the blades for example are modelled by 10 bodies each. If only one body per blade is used the code will become as a linear code since the beam model in each body is linear, whereas a convergence study has shown that with 10 bodies the geometric non-linearities are captured. In the present model, only one blade is considered and modelled as a flexible beam. For first and second modes of blade motions, as considered in this paper, the rotary and shear effects are negligible, so the Bernoulli–Euler beam model in the present mode is comparable with the Timoshenko beam model in HAWC2. As for higher order modes of motion and other turbine components, the rotary and shear effects are of higher relevance. Figure 1 shows the blade flapwise and edgewise deflections and angle of attack at radius 55.5 m (88% blade length) at different wind speeds. The angle of attack indicates how well the torsional deformation from the two models agrees. It is seen that there is good agreement between the present second-order Bernoulli–Euler blade model and HAWC2 for all operational conditions. The kink at rated wind speed ($\approx$11 m s^{-1}) at the blade tip deflection curve is caused by the shift from variable speed, constant pitch to constant speed, variable pitch operation.

4. AEROELASTIC MODES OF BLADE MOTION

In this section, the aeroelastic modes of blade motion are analysed with particular emphasis on effects of steady-state flapwise blade deflection. The stability of a specific blade at normal operation will be analysed in detail and differences including and excluding geometric couplings will be discussed. The effect of pre-bend is similar to the effects of steady-state blade deflection which is investigated in this analysis. The effect of sweep (edgewise curved blades) is different since it couples flapwise and torsional motion instead of edgewise and torsion as characterized by the flapwise deflection.

4.1. Linear aeroelastic model

The non-linear partial differential equations of motion is linearized by inserting $\mathbf{u}(s, t) = \mathbf{u}_0(s) + \varepsilon\mathbf{u}_1(s, t)$ into equation (1), where $\mathbf{u}_0(s)$ is the steady-state deflected blade position including any pre-bend and sweep, $\mathbf{u}_1(s, t)$ is time-dependent variations around this position and ε is a bookkeeping parameter denoting smallness of terms. The external influences, such as wind speed, pitch setting, etc. are split into a steady part and a time-varying part (denoted by the subscript 0 and 1, respectively) with the bookkeeping parameter ε. The equation of motion (equation (1)) is Taylor expanded assuming $\varepsilon << 1$. Balancing terms of order ε^1 give the linear approximation around the deflected blade position $\mathbf{u}_0$. By linearizing the equations of motion about the deflected blade the main effects for the geometric non-linearities are preserved. For example, the non-linear stiffness term in the edgewise equation

$$\left((EI_\xi - EI_\eta)\cos\left(\tilde{\theta}+\theta\right)\sin\left(\tilde{\theta}+\theta\right)v''\right)'' \tag{7}$$

becomes

$$\left((EI_\xi - EI_\eta)\cos\left(2\left(\tilde{\theta}+\theta_0\right)\right)v_0''\theta_1\right)'' + \ldots \tag{8}$$

when linearized about the deflected blade (using $\theta = \theta_0 + \theta_1$ and $v = v_0 + v_1$), whereby the important coupling between edgewise and torsional blade motion of a flapwise deflected blade is preserved. The subscript 1 denotes the linear variation around the linearization point u_0. Likewise the non-linear term in the torsional equation

$$(EI_\xi - EI_\eta)\cos\left(2\left(\tilde{\theta}+\theta\right)\right)u''v'' \tag{9}$$

becomes

$$(EI_\xi - EI_\eta)\cos\left(2\left(\tilde{\theta}+\theta_0\right)\right)u_0''u_1'' + \ldots \tag{10}$$

when linearized about the deflected blade. The major effect of the important geometric coupling in the stiffness terms (equations (7) and (9)) between edgewise and torsional motion of a flapwise deflected blade is preserved when linearized about the steady-state deflected blade (equations (8) and (10)).

The linearized equations of motion are combined with a linearized Beddoes–Leishman[27] type of unsteady aerodynamic model.[25] The unsteady aerodynamic model is formulated in a state space formulation with four states; two states are second-order approximations to Thoedorsen's function[28] and two states describe the dynamics of the trailing edge separation point. Periodic effects, such as gravity, can be included in the linear model by considering $\sin(\phi_1 + t\dot{\phi}_0)$ and $\cos(\phi_1 + t\dot{\phi}_0)$ as independent variables, which subsequently can be obtained by a non-linear transformation, but are neglected in this work. The linear partial differential equation and the unsteady aerodynamic model are given by

$$\begin{aligned}\tilde{\mathbf{M}}\ddot{\mathbf{u}} + \tilde{\mathbf{D}}\dot{\mathbf{u}} + \left(\tilde{\mathbf{K}}_{ss}\mathbf{u}''\right)'' + \left(\tilde{\mathbf{K}}_{s}\mathbf{u}'\right)' + \tilde{\mathbf{K}}\mathbf{u} + \tilde{\mathbf{C}}\mathbf{z} &= \tilde{\mathbf{F}}_s\tilde{\mathbf{f}} \\ \dot{\mathbf{z}} + \tilde{\mathbf{T}}\mathbf{z} + \tilde{\mathbf{G}}\ddot{\mathbf{u}} + \tilde{\mathbf{H}}\dot{\mathbf{u}} + \tilde{\mathbf{J}}\mathbf{u} &= \tilde{\mathbf{F}}_a\tilde{\mathbf{f}}\end{aligned} \tag{11}$$

where $\mathbf{u} = \mathbf{u}(s, t) = [u_1(s, t), v_1(s, t), \theta_1(s, t)]$ are the linear deflections around the linearization point $\mathbf{u}_0$, $\tilde{\mathbf{M}} = \tilde{\mathbf{M}}(\mathbf{u}_0, \dot{\phi}_0, \beta_0, U_{n,0})$, $\tilde{\mathbf{D}} = \tilde{\mathbf{D}}(\mathbf{u}_0, \dot{\phi}_0, \beta_0, U_{n,0})$, $\tilde{\mathbf{K}}_{ss} = \tilde{\mathbf{K}}_{ss}(\mathbf{u}_0, \dot{\phi}_0, \beta_0)$, $\tilde{\mathbf{K}}_s = \tilde{\mathbf{K}}_s(\dot{\phi}_0, \beta_0)$, $\tilde{\mathbf{K}} = \tilde{\mathbf{K}}(\mathbf{u}_0, \dot{\phi}_0, \beta_0, U_0)$ are collections of the linear coefficients, where U_0 is the mean wind speed, $\tilde{\mathbf{C}} = \tilde{\mathbf{C}}(\mathbf{u}_0, \dot{\phi}_0, \beta_0)$ is the unsteady aerodynamic's effect on the structure, where U_1 is the variation of the wind speed. The coupling to external influences such as pitch action and wind speed variations is described on the right hand side, where $\tilde{\mathbf{F}}_s = \tilde{\mathbf{F}}_s(\mathbf{u}_0, \dot{\phi}_0, \beta_0, U_{n,0})$ holds the linear gains on the external influences given by $\tilde{\mathbf{f}} = [\beta(t), \dot{\beta}(t), \ddot{\beta}(t), \sin(\phi_1(t) + t\dot{\phi}_0), \cos(\phi_1(t) + t\dot{\phi}_0), \dot{\phi}_1(t), \ddot{\phi}_1(t), U_1(s, t), \dot{U}_1(s, t)]^T$. The four aerodynamic states in $\mathbf{z}$ are modelled by steady-state wind speed-dependent time constants $\tilde{\mathbf{T}}$ and affected by the linear blade deflection, speed and acceleration through time-varying angle of attack and local wind speed described by the matrices $\tilde{\mathbf{G}}$, $\tilde{\mathbf{H}}$ and $\tilde{\mathbf{J}}$.[25] The linear gains on external influences are given by $\tilde{\mathbf{F}}_a$.

4.2. Aeroelastic modes of motion

The spatial derivatives in the linear equations of aeroelastic motion (equation (11)) are approximated by the finite difference scheme (Table I) with N discretization points. The finite difference implementation includes the spatial boundary conditions (equations (4) and (5)). The second-order differential equation is then rewritten into first-order form by introducing the first-order time derivatives as states and combining it with the unsteady aerodynamic model. The spatial discretized first-order equation of aeroelastic motion becomes

$$\dot{\mathbf{x}} = \mathbf{A}\mathbf{x} + \mathbf{B}\mathbf{f} \tag{12}$$

where $\dot{\mathbf{x}}$ includes the linear deformation around the linearization point, speed and the aerodynamic states for each discretization point, giving $3N + 3N + 4N = 10N$ degrees of freedom, $\mathbf{A}$ is the linear coefficients, $\mathbf{B}$ is the linear gains on the external influences and $\mathbf{f}$ is the linear variation of the external influences. The unforced version of equation (12) forms a differential eigenvalue problem.[29] The differential eigenvalue problem is casted into an algebraic eigenvalue problem by assuming a complex exponential solution. The eigenvalues and corresponding eigenvectors can be grouped into two sets: real valued and complex valued eigenvalues. Generally, the real valued eigenvalues are related to the aerodynamic states and correspond to the aerodynamic time lags. However, overdamped aeroelastic modes will also have real valued eigenvalues. The complex valued eigenvalues are related to the aeroelastic states and give the aeroelastic frequencies and damping. The corresponding eigenvectors give the aeroelastic mode shapes of the particular mode.

It is noted that since aerodynamic forces are included, the eigenvalue problem[12] is not self-adjoint, and therefore, the eigenvectors are not orthogonal.

Wind Energ. 2011; **14**:209–224 © 2010 John Wiley & Sons, Ltd.
DOI: 10.1002/we

4.3. Frequency and damping of a blade at normal power production conditions

The model described above is used to analyse the effect of geometric non-linearities caused by steady-state blade deflections under normal operational conditions. The aeroelastic frequencies, damping and mode shapes of the NREL RWT blade are computed for different wind speeds in the power production region. The aeroelastic results are computed in two versions: one in which the model is linearized about the steady-state deflected blade, and another in which it is linearized about the undeflected blade, hereby including and excluding the effect of the geometric non-linearities, respectively.

The results from the present model are compared with the results from the non-linear aeroelastic time simulation code HAWC2. Since each body in this code is a linear beam model and the non-linearities are only included by the multi-body formulation, this model will produce linear results if only one body per blade is used and non-linear results if more bodies are used. Hence, a one body per blade model will correspond to the present model without geometric couplings and a model with more bodies will correspond to the present model with geometric couplings. Two versions of the HAWC2 model are used in this work: one with one body in the blade and one with 10 bodies in the blade. In both models, only the blade is considered as a flexible beam. The frequencies and damping from the time simulation code are estimated by fitting the frequency, phase and damping of a number of exponentially decaying sinusoidal functions to the decay of the blade motion after an initial excitation at the expected aeroelastic frequency. In the simulations, the pitch angle is set to a prescribed value dependent on wind speed only.

Figure 2 shows the aeroelastic frequencies and damping of the two first flapwise blade-bending modes. In the variable speed operation range (5 to 12 m s^{-1}), the aeroelastic frequency increases because of increased centrifugal stiffness. The disagreement between the undeflected and deflected blade case in aeroelastic frequency of the first flapwise mode around 20 m s^{-1} is caused by the increased steady-state blade twist, which changes the angle of attack and thereby the aerodynamic stiffness. The damping of the first flapwise bending mode is almost the same for the undeflected and deflected blade case, there are only some minor differences at the same wind speeds that are also caused by the small change in steady angle of attack. For the second flapwise bending mode, neither the frequency nor the damping are changed by the inclusion of the geometric non-linearities. The results for the second flapwise mode from HAWC2 are seen to follow the same trend as the results from the present model. Because of the high damping of this mode, the decay of initial excited oscillations is very fast and the noise from other lower damped modes becomes relatively large, resulting in a large uncertainty on the fitting of damping to this short decay time. The geometric non-linearities do not have a large effect on the flapwise bending modes since the edgewise steady-state deflection is relatively small, giving only a weak coupling from flapwise motion to the other directions.

Figure 3(a) shows the aeroelastic frequencies and damping for the first edgewise blade-bending mode. There is an offset of the frequency of the two different models (HAWC2 and the present model). The reason for this offset is that the present model only includes the blade whereas the HAWC2 model includes the whole turbine. The turbine's effect on the blade dynamics is minimized by making all other turbine components very stiff in the HAWC2 computations, but nonetheless there will always be a small effect. This effect is more pronounced for the edgewise mode since the coupling is more direct through the drive train and the other blades than it is for the flapwise mode. The change in frequency caused by the blade deflection is also seen to have a minor difference in offset for the two models. This is due to the fact that in the

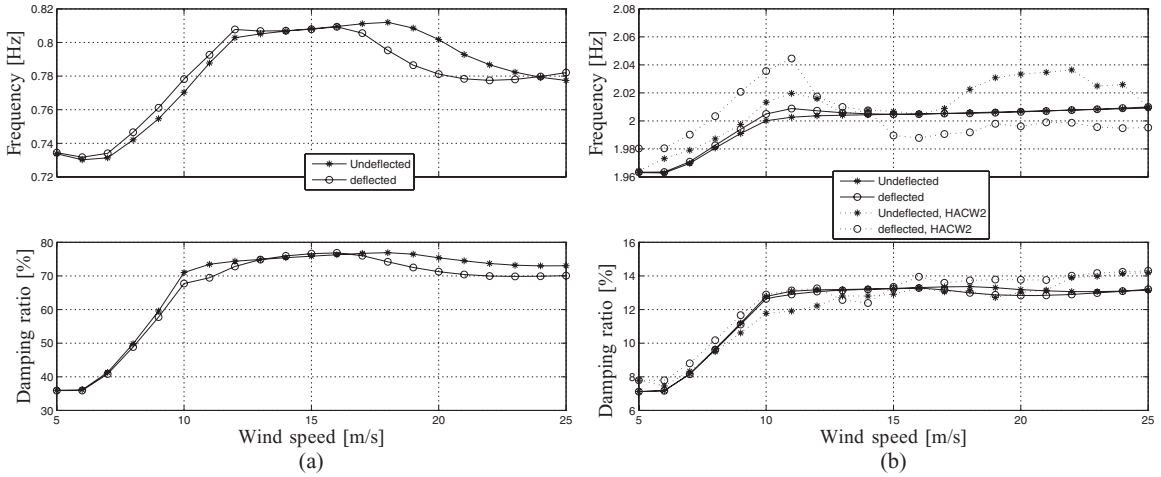

Figure 2. Aeroelastic frequency and damping for the (a) first and (b) second flapwise blade-bending modes. There are no HAWC2 results for first flapwise mode because it is too highly damped for measuring the decay.

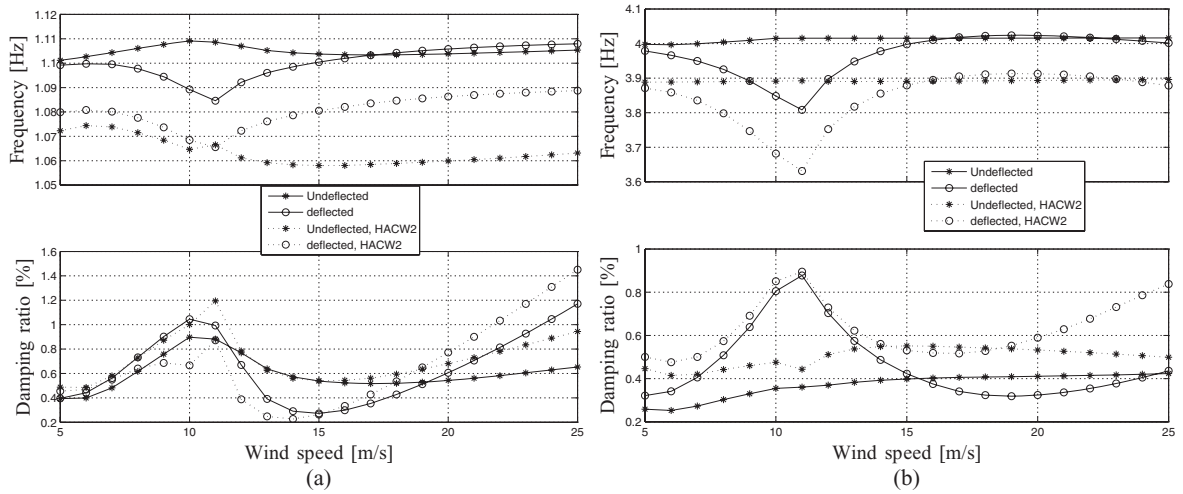

Figure 3. Aeroelastic frequency and damping ratio for (a) the first and (b) the second edgewise blade-bending modes. Damping ratio refers to the exponential damping rate.

HAWC2 model the aerodynamic forces are applied to the deformed blade position even if the blade is assumed linear whereas in the present model the forces are applied to the undeflected blade position. Regardless of these differences, the damping of the two models is qualitatively similar, and since the focus of this work is the qualitative effect of geometric couplings on the blade stability, the present model is well suited for this purpose. The aeroelastic damping around 14 m s^{-1} decreases when the geometric non-linear couplings are included (deflected blade case). At the higher wind speeds, the damping of the model including the geometric non-linearities increase and becomes the highest. The reason for these differences will be analysed in the next section. Figure 3(b) shows the aeroelastic frequency and damping of the second edgewise bending mode. The frequency and damping from the present model differ from the results from HAWC2 at a wind speed around 11 m s^{-1}, where the flapwise deflection is largest. This case will be analysed in the next section.

4.4. Aeroelastic analysis of specific cases

The aeroelastic damping of the edgewise mode is a caused by both flapwise and edgewise aerodynamic force variations, which results from angle off attack variations due to edge-torsion coupling of the flapwise deflected blade and from flap and edgewise blade motion. On the one hand, modal aerodynamic force variation that occurs in counter phase with the blade speed enhances the damping. On the other, when it is in-phase with speed, the damping decreases or even becomes negative. When modal aerodynamic force variations are in counter phase with the blade deflection, aerodynamic stiffening occurs and vice versa. The following discussion is clarified through phase-space plots of flapwise and edgewise deflections; these phase-space plots also include distinct values of the belonging aerodynamic flapping force variation through a scaled stem-like plot (vertical bars with an o-mark; sign from up/down orientation relative to trajectory). Furthermore, the elastic twist of the blade is included in a distinct number of points of the trajectory in the phase-space plot through a straight, mainly horizontally directed bar. The torsion will increase the angle of attack when the bar is decreasing from left to right and vice versa. The plots are included to clarify the aeroelastic damping mechanisms and to illustrate the difference for an undeflected and a deflected blade. The three cases where there are large differences between the deflected and undeflected blade cases are analysed in detail; the first edgewise bending mode at 14 and 25 m s^{-1} and the second edgewise bending mode at 11 m s^{-1}. **Summary**: In the first cases (first edgewise bending mode at 14 m s^{-1}), the damping of the deflected blade is lower than the damping of the undeflected blade. The damping decreases because the inclusion of geometric non-linearities reduces the flapwise motion and the phase between flapwise motion and flapwise forces is changed. In the second case (first edgewise bending mode at 14 m s^{-1}), the damping of the deflected blade is highest. The increased damping is due to the fact that the geometric non-linearities increase the torsional motion, and thereby the changes in angle of attack and thus the aerodynamic forces. The change in phase and amplitude of the aerodynamic forces relative to the edgewise motion increase the negative aerodynamic work, increasing damping. In the last case (second edgewise bending mode at 11 m s^{-1}) relative large increase in damping is seen when the deflections are included. The increase is caused by an increased amount of torsional motion and negative aerodynamic work on the torsional motion.

Wind Energ. 2011; **14**:209–224 © 2010 John Wiley & Sons, Ltd.
DOI: 10.1002/we

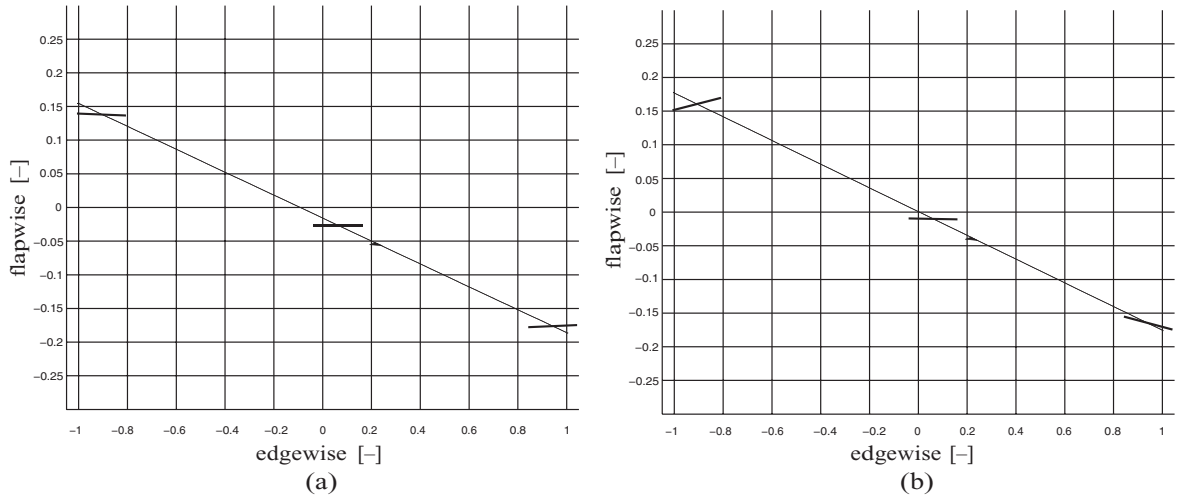

Figure 4. Traces of cross-sectional blade motion at 90% radius in the first structural edgewise eigenmode at 14 m s^{-1} for the blade with exaggeration of the torsional component. Arrows denote the direction of motion and the bars denote the torsional component. (a) Steady-state blade deflection terms are excluded and (b) steady-state blade deflection terms are included. Note that the relative wind comes from right to left in the displayed cross-sectional coordinate system.

The first case to be analysed is the aeroelastic response of the first edgewise blade-bending mode at 14 m s^{-1}, where the deflected blade cases are less damped than the undeflected blade case (Figure 3(a)). First, looking at the case without steady-state blade deflections, which for this blade without pre-bend and sweep will mean a straight blade removing geometric non-linearities: Figure 4 shows the normalized cross-sectional blade deflection at 90% radius for the first edgewise bending structural eigenmodes for the undeflected blade and the steady-state deflected blade at 14 m s^{-1}. When the blade moves forward (left to right) in the structural eigenmode, the local wind speed increases, consequently increasing the aerodynamic forces, and vice versa when the blade moves backwards. The extremes of this variation of aerodynamic forces appear at the points with the largest blade speed, i.e. the midpoint of the edgewise blade motion. The flapwise motion in the structural eigenmode also affects the aerodynamic force, increasing the angle of attack when the blade moves downwards and thereby increasing the aerodynamic force. Since the edgewise and flapwise motion are in counter phase (blade moves forward and downwards) in this structural eigenmode, both effects described above give the highest aerodynamic forces when the blade moves forward and lowest when the blade moves backwards. In this case, without steady-state deformations, there is only a very limited and insignificant torsional motion. The variations in aerodynamic flapwise forces affect the flapwise motion in the aeroelastic mode of motion. The frequency of the first edgewise mode (1.1 Hz) is higher than the resonance frequency of first flapwise bending mode (0.79 Hz). Hence, the flapwise deflection lags approximately 180 degrees after the flapwise force according to basic dynamic considerations. The flapwise force is highest at the midpoint of the forward edgewise motion, increasing the flapwise deflection around the midpoint of the backward edgewise motion. This increased flapwise motion at the midpoint of the edgewise motion will increase the flapwise speed at the edgewise turning points, affecting the angle of attack and thereby the aerodynamic force. The increased flapwise forces will increase the flapwise deflection ≈180 degrees later, which is the other edgewise turning point. Summing up, the flapwise motion in the first edgewise aeroelastic bending mode is an equilibrium between the flapwise motion caused by the structural coupling (eigenmode motion) and the variations in flapwise aerodynamic force caused by the structural eigenmode and the flapwise motion itself. Figure 5(b) shows the unsteady aerodynamic flapwise force for the cross-sectional motion of first edgewise aeroelastic bending mode. The resulting aerodynamic flapwise force variation is seen to be largest around the edgewise turning points, indicating that it is dominated by the force variation caused by the flapwise motion itself. The black dot denotes the point with the largest flapwise force.

Figure 6(b) shows the change in cross-sectional motion caused by the aerodynamic forces. It is seen that the largest flapwise deflection caused by the aerodynamic forces is ≈180 degree offset from the largest flapwise force.

When the steady-state deflections are included in the model, the geometric non-linear couplings between edgewise and torsional motion of a flapwise deflected blade (equations (8) and (10)) become active and increase the torsional motion in the first flapwise structural eigenmode (Figure 4(a)). The torsional motion is seen to decrease the angle of attack, and thereby the aerodynamic force, at the forward position of the edgewise motion so this torsional motion counteracts the angle of attack changes caused by the flapwise speed at the edgewise turning points. The reduced effect of the flapwise motion on the aerodynamic forces changes the phase between flapwise and edgewise motion. The flapwise motion

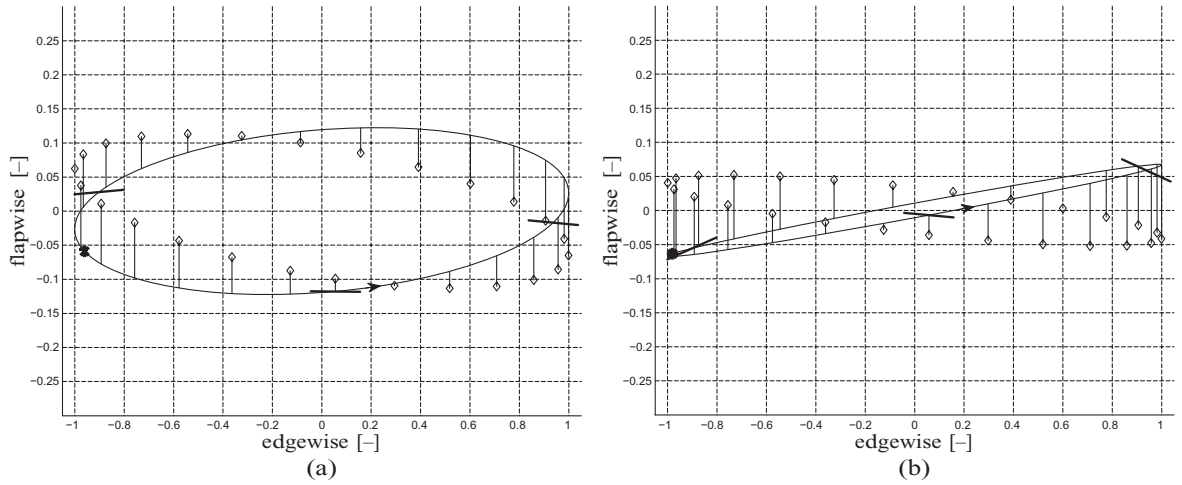

Figure 5. Traces of cross-sectional blade motion at 90% radius in the first aeroelastic edgewise mode at 14 m s^{-1} for the blade with exaggeration of the torsional component. Arrows denote the direction of motion, the bars denote the torsional component and the vertical lines the unsteady flapwise aerodynamic force with the black dot at the point with highest force. (a) Steady-state blade deflection terms are excluded and (b) steady-state blade deflection terms are included. Note that the relative wind comes from right to left in the displayed cross-sectional coordinate system.

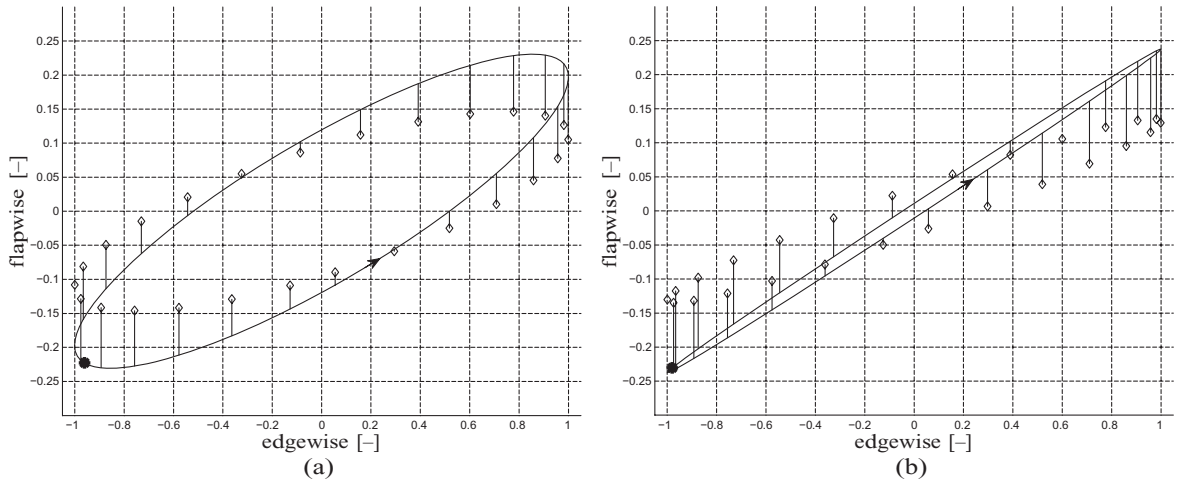

Figure 6. Change in cross-sectional blade motion at 90% radius of the first aeroelastic edgewise mode at 14 m s^{-1} caused by aerodynamic forces. The figure shows the difference between the structural eigenmode (Figure 4) and the aeroelastic mode (Figure 5) showing that the maximum flapwise deflection caused by aerodynamic forces are 90 degrees phase shifted from the maximum force. Arrows denote the direction of motion and the vertical lines the unsteady flapwise aerodynamic force with the black dot at the point with highest force. (a) Steady-state blade deflection terms are excluded and (b) steady-state blade deflection terms are included. Note that the relative wind comes from right to left in the displayed cross-sectional coordinate system.

relative to the local wind becomes smaller but only looking at the change in flapwise motion caused by aerodynamic forces (Figure 6) the deflections are similar, so it is mainly the phase between flapwise and edgewise motion that has changed.

Table II shows the aerodynamic sectional work for the two cases in Figure 5. Both the flapwise and edgewise aerodynamic works are seen to be negative, thus extracting energy from the motion (adding damping to the mode). For the undeflected blade case, the total work is dominated by the flapwise work. The relatively high flapwise work is due to the fact that the flapwise force is ≈90 degrees phase shifted from the flapwise motion, so for this reason the largest forces counteract at the highest velocities. The flapwise force is mainly caused by the flapwise component of the lift force on the airfoil. This lift force will also have an edgewise component pointing forward (the component driving the wind turbine)

Wind Energ. 2011; **14**:209–224 © 2010 John Wiley & Sons, Ltd.
DOI: 10.1002/we

Table II. Aerodynamic sectional work for the sectional motion shown in Figure 5. The work is normalized with respect to the total work of the undeflected blade, except for the sign.

	Edgewise	Flapwise	Total
Undeflected blade	−0.03	−0.97	−1.00
Deflected blade	−0.25	−0.27	−0.52

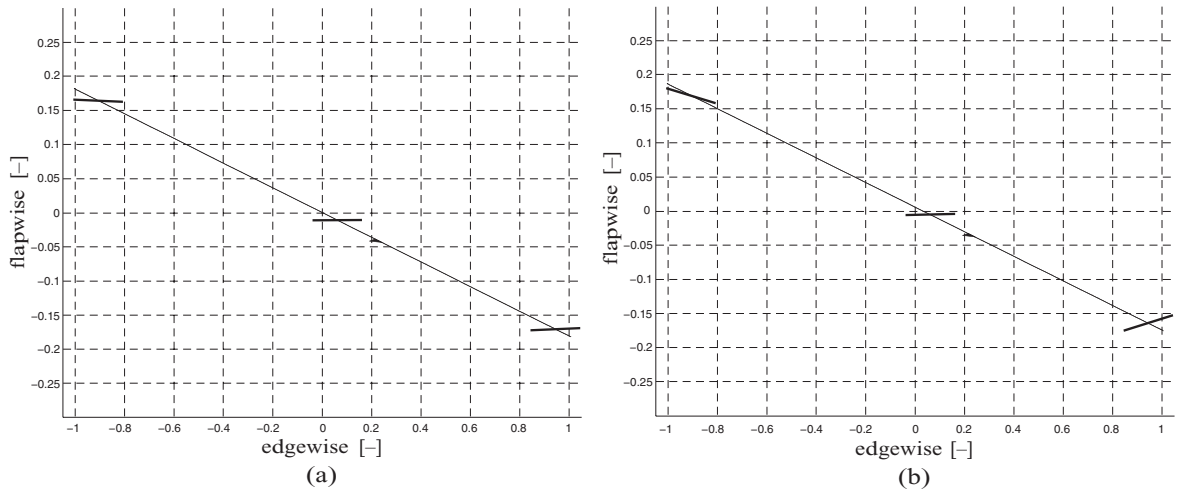

Figure 7. Traces of cross-sectional blade motion at 90% radius in the first structural edgewise eigenmode at 25 m s^{-1} for the blade with exaggeration of the torsional component. Arrows denote the direction of motion and the bars denote the torsional component. (a) Steady-state blade deflection terms are excluded and (b) steady-state blade deflection terms are included. Note that the relative wind comes from right to left in the displayed cross-sectional coordinate system.

so the point with the highest flapwise force also has a relatively large edgewise force component pointing forward. For the undeflected blade case (Figure 5(b)), the blade moves forward at the point with the highest forces. Consequently at this point, the edgewise component of the lift will add energy to the system, reducing the damping. This is the reason for the low damping value for the edgewise motion of the undeflected blade (Table II). In the deflected blade case, two effects reduce the flapwise damping: first, the reduced flapwise motion relative to the local wind, reduces the amount of work. Second, the flapwise force and motion are almost in counter phase, so the maximum forces act at a low flapwise velocity, extracting less energy from the system. The edgewise work is increased since the point of maximum force is moved towards the edgewise turning point compared with the undeflected blade case, which reduces the amount of energy that the lift force component on the edgewise motion adds to the system, leading to a higher edgewise damping contribution (Table II).

The next case to be analysed is the first edgewise blade-bending mode at 25 m s^{-1} where the damping of the deflected blade is higher than the damping of the undeflected blade case (Figure 3(a)). At this higher wind speed, the flapwise tip deflection shifts sign (Figure 1) changing the sign of the coupling between edgewise and torsional motion for the flapwise deflected blade (equations (8) and (10)). Figure 7 shows how the torsional deflection in the first edgewise structural eigenmode at 25 m s^{-1} has changed sign compared with the results for 14 m s^{-1} (Figure 4). Figure 8 shows the cross-sectional deflection of the first edgewise aeroelastic mode and the unsteady aerodynamic flapwise forces at 25 m s^{-1}. At this wind speed, the average angle of attack at the shown cross-section is ≈−4 degrees. At this negative angle of attack, the lift force is negative, so the effect of edgewise vibration change, since the forward motion, which gives larger local wind speed, increases the absolute value of the negative lift force. Hence, the forward motion decreases the lift and the backward motion increases the lift, opposite the case at 14 m s^{-1}. The effect of flapwise motion is the same as before since this affects the angle of attack. So the two effects counteract each other, resulting in smaller unsteady aerodynamic forces in this mode at 25 m s^{-1} than at 14 m s^{-1} (Figure 8). The phase between the flapwise and edgewise motion determines how well the forces from the two effects cancel each other out and thereby also where the highest force appears. Because of the reduced aerodynamic forces, the aeroelastic mode is less affected by the aerodynamic forces and the direction of motion is similar to the structural eigenmode when compared with the previous case at 14 m s^{-1}. The edgewise force is mainly caused by the lift force on the blade, and since the angle of attack in this 25 m s^{-1} case is negative

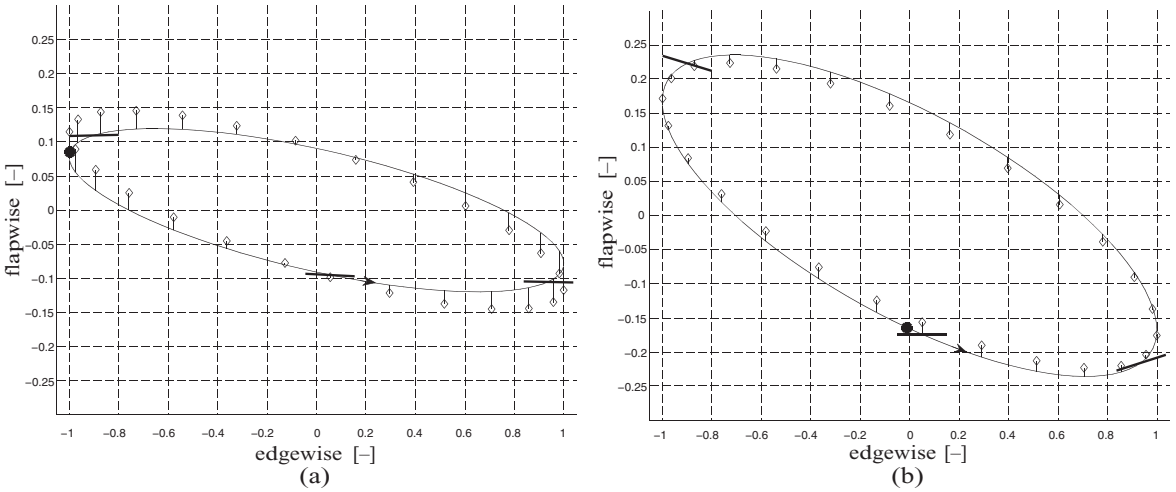

Figure 8. Traces of cross-sectional blade motion at 90% radius in the first aeroelastic edgewise mode at 25 m s^{-1} for the blade with exaggeration of the torsional component. Arrows denote the direction of motion, the bars denote the torsional component and the vertical lines the unsteady flapwise aerodynamic force with the black dot at the point with highest force. (a) Steady-state blade deflection terms are excluded and (b) steady-state blade deflection terms are included. Note that the relative wind comes from right to left in the displayed cross-sectional coordinate system.

Table III. Aerodynamic sectional work for the sectional motion shown on Figure 8. The work is normalized with respect to the total work of the undeflected blade, except for the sign.

	Edgewise	Flapwise	Total
Undeflected blade	−0.56	−0.44	−1.00
Deflected blade	−1.13	−0.43	−1.57

(≈−4 degrees), a lift force giving a positive flapwise force will give a negative edgewise force. Thus, for the first ≈2/3 for the forward and backward edgewise motion, the aerodynamics will contribute with negative work (Figure 8(b)). For the flapwise motion, the flapwise force is almost constantly in the opposite direction than the flapwise motion, extracting energy from the motion. Table III shows that the flapwise and edgewise works contribute equally to the damping of the undeflected blade case at 25 m s^{-1}. The changes in blade twist, and thereby angle of attack, caused by the geometric non-linearities increase the aerodynamic force at the forward edgewise position of the blade and decreases the forces at the backward position. Adding this extra effect to the effects of flapwise and edgewise motion moves the point of highest flapwise force towards the forward position and places it almost at the midpoint for both the flapwise and edgewise motion. Having the highest flapwise force (indicating high negative edgewise force at this negative angle of attack) close to the highest flapwise and edgewise speed, results in high damping even though the force level is relatively low.

The last case to be analysed is the second edgewise blade-bending mode at 11 m s^{-1}, where the damping of the deflected blade case is much higher than the damping of the undeflected blade case (Figure 3(b)). On a pitch-regulated wind turbine, as the present one, the flapwise tip deflection is largest around rated wind speed since the pitch regulation of the turbine relieves the aerodynamic loads at higher wind speeds. The large flapwise steady-state deflection (indicating large curvature $v_0'' \propto v_0$) together with the relatively large edgewise curvature u_1'' gives a large torsional component in the second edgewise bending mode (equation (10)). Figure 9 shows the content of flapwise, edgewise and torsional motion in the second edgewise bending mode and it is seen how the inclusion of the non-linearities increases the torsional motion. Figure 10 shows the distribution of aerodynamic work done by the edgewise, flapwise and torsional aerodynamic forces along the blade. It is on the outer 10% of the blade, beyond the node of the second bending mode, that the majority of the aerodynamic work is done and the difference between the two blade deflection cases arises. The main differences in aerodynamic work between undeflected and deflected blade cases are in the torsional motions, which increase when the geometric non-linearities are included. Figure 11 shows the cross-sectional motion for the second aeroelastic edgewise bending mode for the undeflected and the deflected blade at 95% blade radius. The modal aeroelastic cross-sectional motion of the undeflected blade is very similar to the structural eigenmode: this is because the unsteady aerodynamic

Wind Energ. 2011; **14**:209–224 © 2010 John Wiley & Sons, Ltd.
DOI: 10.1002/we

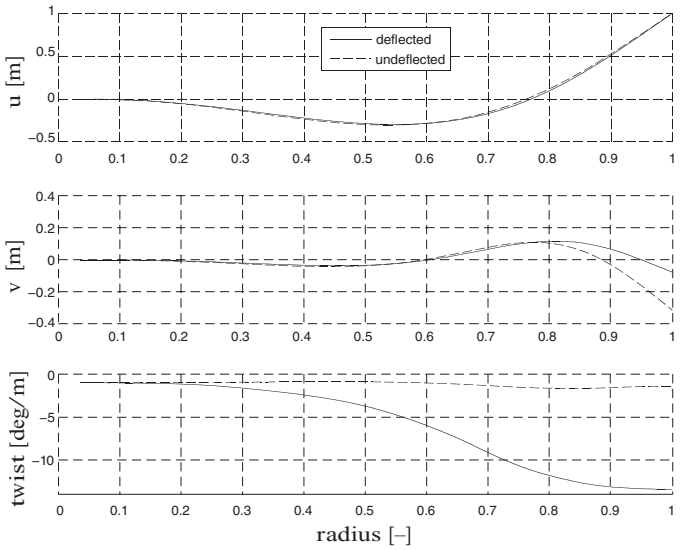

Figure 9. Edgewise, flapwise and torsional components of the second edgewise aeroelastic bending mode at 11 m s^{-1} for the undeflected and the deflected blade.

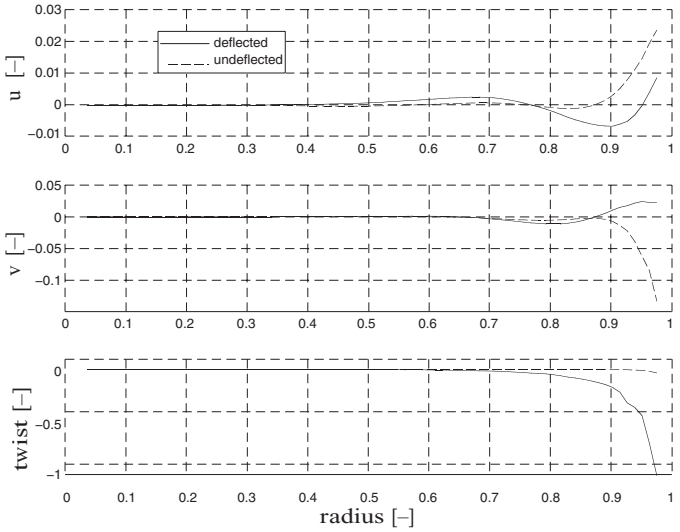

Figure 10. Edgewise, flapwise and torsional cross-sectional work in the second edgewise aeroelastic vibration mode at 11 m s^{-1} for the undeflected and the deflected blade. Negative aerodynamic work corresponds to positive aeroelastic damping.

forces are smaller relative to the higher inertia and structural restoring forces in this higher bending mode compared with the first edgewise mode. Figure 10 shows that the edgewise motion is slightly negatively damped for the outer part of the blade. This is because the edgewise component of the unsteady lift force acts in the direction of edgewise motion adding energy to the system. This results in minor negative damping because the drag force on the edgewise motion always adds damping. The flapwise motion is positively damped since the unsteady flapwise force works against the direction of flapwise motion.

When the steady-state deflections are included, the large torsional component caused by the geometric non-linearities (equation (10)) has a large effect on the unsteady aerodynamic forces. Note that the direction of the loop has changed compared with the undeflected blade case. The edgewise force adds energy to the system, since the force acts in the same direction and the motion for the first ≈2/3 of the edgewise motion. The flapwise forces in the deflected blade case add energy to the system (Figure 10) since they act in the same direction as the flapwise motion. The amount of work is relatively small because the flapwise amplitude normal to the local wind direction is relatively small. The large increase

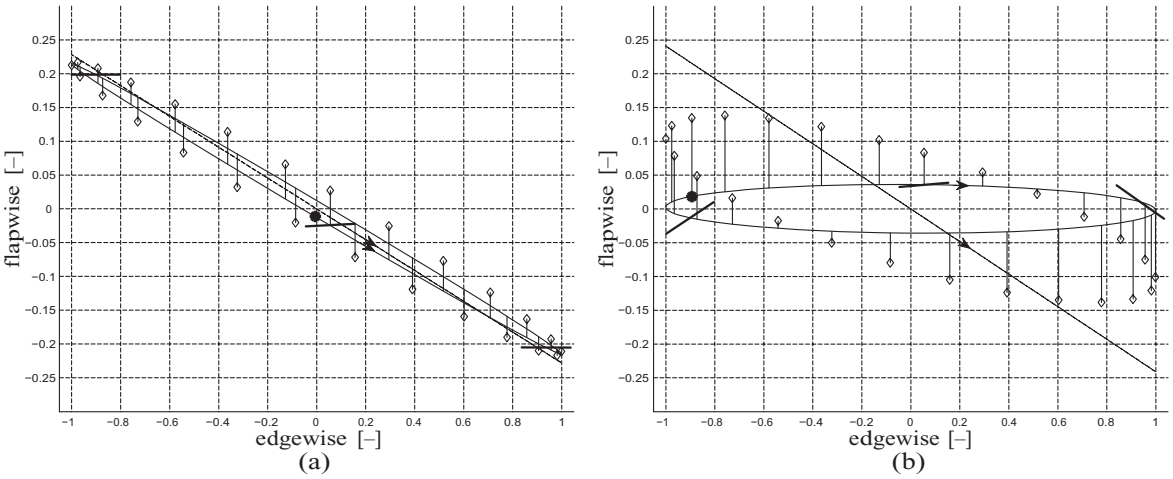

Figure 11. Traces of cross-sectional blade motion at 95% radius in the second aeroelastic edgewise mode at 11 m s^{-1} for the blade with exaggeration of the torsional component. Arrows denote the direction of motion, the bars denote the torsional component and the vertical lines the unsteady flapwise aerodynamic force with the black dot at the point with highest force. The dotted line shows the structural eigenmode. (a) Steady-state blade deflection is excluded and (b) steady-state blade deflection is included. Note that the relative wind comes from right to left in the displayed cross-sectional coordinate system.

in aeroelastic damping of the deflected blade case compared with the undeflected blade case is caused by negative aerodynamic work of the torsional motion (Figure 10). The aerodynamic lift force acts at the aerodynamic centre, which is located in front of the elastic centre, where the blade twists. Thus, an increased lift results in an increased rotational moment on the cross-section. The cross-sectional motion of the undeflected blade (Figure 11(b)) has almost no torsional motion, resulting in small aerodynamic work (Figure 10). The deflected blade case, on the other hand, has much more torsional motion (Figure 11(b)). The cross-section has a nose down motion on its way forward to the lift force and thereby also the torsional moment is high and a nose up motion on its way back where the lift is low, resulting in negative aerodynamic work, increasing the damping.

5. CONCLUSION

In this paper, a second-order non-linear beam model is used for aeroelastic stability analysis of a turbine blade. The aeroelastic mechanisms of the different modes and the difference between including and excluding non-linear geometric couplings caused by steady-state deflection at normal operation are discussed in detail. The methodology can also be used to analyse the effects of pre-bend or swept blades.

The analysis is based on the non-linear structural blade model from Kallesøe,[23] which in this work is extended to include an aerodynamic model. The resulting non-linear aeroelastic blade model is linearized about a curved blade position, caused by e.g. sweep, pre-bend or steady-state deflections. The linearized model is used to perform stability analysis of a steady-state deflected blade and to examine the effects of the linearized geometric non-linearities.

First, the derived non-linear aeroelastic model is used to compute steady-state blade deflections. The steady-state deflections are validated against results from a non-linear aeroelastic time simulation code, showing good agreement. Next, the non-linear aeroelastic model is linearized about the steady-state deflected blade. By linearizing about the deflected blade, the main effects of geometric non-linearities are preserved and the results show how the relative large flapwise blade deflection introduces a coupling between edgewise and torsional blade motion.

Two versions of the linearized model are used to compute the aeroelastic stability of the blade: one linearized about the deflected blade, preserving the non-linearities and one linearized about an undeflected blade excluding the non-linearities. The stability results from the two versions are compared and the differences discussed. It is found that the flapwise modes are not as affected by the steady-state blade deflection as the edgewise modes. The damping of first edgewise bending mode of the steady-state deflected blade decreases around 14 m s^{-1} but increases around 25 m s^{-1} compared with the undeflected blade. The reason for this change of the effect of the blade deflection on the aeroelastic damping is caused by the steady-state flapwise deflection shifting sign around 20 m s^{-1}. When the flapwise deflection shifts sign, the coupling between the edgewise and torsional motion also shifts, and thereby changing the non-linear geometric couplings effect on the aeroelastic damping contribution. The damping of second edgewise bending mode is

Wind Energ. 2011; **14**:209–224 © 2010 John Wiley & Sons, Ltd.
DOI: 10.1002/we

high around 11 m s^{-1} for the steady-state deflected blade compared with the undeflected blade. This is because the flapwise steady-state deflection is largest around 11 m s^{-1} giving the largest effect of the geometric non-linear coupling between edgewise and torsional motion.

This work shows that the blade deflection under normal operation conditions affects the aeroelastic stability properties of the blades. In the worst case for this particular blade, the edgewise damping can be decreased by half.

REFERENCES

1. Hodges DH, Dowell EH. Nonlinear equations of motion for the elastic bending and torsion of twisted nonuniform rotor blades. *Technical Report* TN D-7818, NASA, 1974.
2. Friedmann PP, Kottapalli SBR. Coupled flap-lag-torsional dynamics of hingeless rotor blades in forward flight. *Journal of the American Helicopter Society* 1982; **4**: 28–36.
3. Panda B, Chopra I. Flap-lag-torsion in forward flight helicopter. *Journal of the American Helicopter Society* 1985; **30**: 30–39.
4. Crespo da Silva MRM, Hodges DH. Nonlinear flexure and torsion of rotating beams, with application to helicopter rotor blades—II. Response and stability results. *Vertica* 1986; **10**: 171–186.
5. Hodges DH, Saberi H, Ormiston RA. Development of nonlinear beam elements for rotorcraft comprehensive analyses. *Journal of the American Helicopter Society* 2007; **52**: 36–48.
6. Friedmann PP. Aeroelastic stability and response analysis of large horizontal-axis wind turbines. *Journal of Wind Engineering and Industrial Aerodynamics* 1980; **5**: 373–401.
7. Chaviaropoulos PK. Flap/lead-lag aeroelastic stability of wind turbine blades. *Wind Energy—Bognor Regis* 2001; **4**: 183–200.
8. Politis E, Riziotis V. The importance of nonlinear effects identified by aerodynamic and aero-elastic simulations on the 5mw reference wind turbine. *Technical Report*, Center for Renewable Energy Sources, Pikermi, Greece, 2007.
9. Kallesøe BS, Hansen MH. Effects of large bending deflections on blade flutter limits. *Technical Report*, Risøe DTU, Roskilde, Denmark, 2008.
10. Riziotis VA, Voutsinas SG, Politis ES, Chaviaropoulos PK, Hansen AM, Madsen HA, Rasmussen F. Identification of structural non-linearities due to large deflections on a 5mw wind turbine blade. *Proceedings of the EWEC '08, Scientific Track*, Brussels, 2008.
11. van Engelen TG. Control design based on aero-hydro-servo-elastic linear models from turbu (ecn). *Proceedings of European Wind Conference*, Milan, 2007.
12. Riziotis VA, Politis ES, Voutsinas SG, Chaviaropoulos PK. Stability analysis of pitch-regulated, variable-speed wind turbines in closed loop operation using a linear eigenvalue approach. *Wind Energy* 2008; **11**: 517–535.
13. Ashwill TD, Kanaby G, Jackson K, Zuteck M. Development of the swept twist adaptive rotor (star) blade. *Proceedings of the 48th AIAA Aerospace Sciences Meeting Including the New Horizons Forum and Aerospace Exposition*, Orlando, Florida, 2010.
14. Larsen TJ, Hansen A, Buhl T. Aeroelastic effects of large blade deflections for wind turbines. *Proceedings of the Special Topic Conference 'The Science of making Torque from Wind'*, Copenhagen, Denmark, 2004; 238–246.
15. Larsen TJ, Madsen HA, Hansen MA, Thomsen K. Investigations of stability effects of an offshore wind turbine using the new aeroelastic code hawc2. *Proceedings of the Conference 'Copenhagen Offshore Wind 2005'*, Copenhagen, Denmark, 2005.
16. NWTC Design Codes (ADAMS2AD by LainoDJ, Jonkman J). [Online]. Available: http://wind.nrel.gov/designcodes/simulators/adams2ad/ (Accessed 12 August 2005).
17. NWTC Design Codes (AeroDyn by Laino DJ). [Online]. Available: http://wind.nrel.gov/designcodes/simulators/aerodyn/ (Accessed 5 July 2005).
18. NWTC Design Codes (FAST by Jonkman J). [Online]. Available: http://wind.nrel.gov/designcodes/simulators/fast/ (Accessed 12 August 2005).
19. Hansen MH. Improved modal dynamics of wind turbines to avoid stall-induced vibrations. *Wind Energy* 2003; **6**: 179–195.
20. Riziotis VA, Voutsinas SG, Politis ES, Chaviaropoulos PK. Aeroelastic stability of wind turbines: the problem, the methods and the issues. *Wind Energy* 2004; **7**: 373–392.
21. Hansen MH. Aeroelastic stability analysis of wind turbines using an eigenvalue approach. *Wind Energy* 2004; **7**: 133–143.

22. Hansen MH. Aeroelastic instability problems for wind turbines. *Wind Energy* 2007; **10**: 551–577.
23. Kallesøe BS. Equations of motion for a rotor blade, including gravity, pitch action and rotor speed variations. *Wind Energy* 2007; **10**: 209–230.
24. Jonkman J. NREL 5MW baseline wind turbine. *Technical Report*, NREL/NWTC, Golden, Colorado, 2005.
25. Hansen MH, Gaunaa M, Madsen HA. A Beddoes-Leishman type dynamic stall model in state-space and indicial formulation. *Technical Report Risø-R-1354(EN),* Risø National Laboratory, Roskilde, 2004. [Online]. Available: http://www.risoe.dk (Accessed August 2004).
26. Hansen MOL. *Aerodynamics of Wind Turbines*. James & James: Earthscan, London, 2001.
27. Leishman JG, Beddoes TS. A semi-empirical model for dynamic stall. *Journal of the American Helicopter Society* 1989; **34**: 3–17.
28. Thoedorsen T. General theory of aerodynamic instability and the mechanism of flutter. *NACA Report 496*, 1935.
29. Thomsen JJ. *Vibrations and Stability: Advanced Theory, Analysis, and Tools*. Springer-Verlag: Berlin—Heidelberg—New York, 2003.

Wind Energ. 2011; **14**:209–224 © 2010 John Wiley & Sons, Ltd.
DOI: 10.1002/we